Article

A Preliminary Laboratory Evaluation of Artificial Aggregates from Alkali-Activated Basalt Powder

Sergio Copetti Callai [1], Piergiorgio Tataranni [1], Manuel De Rose [2], Annalisa Natali Murri [3], Rosolino Vaiana [2,*] and Cesare Sangiorgi [1]

1   Department of Civil, Chemical, Environmental and Materials Engineering, University of Bologna, 40136 Bologna, Italy
2   Department of Civil Engineering, University of Calabria, Arcavacata Campus, 87036 Rende (CS), Italy
3   CNR–ISTEC Institute of Science and Technology for Ceramics, 48018 Faenza, Italy
*   Correspondence: rosolino.vaiana@unical.it

Abstract: The widespread use of natural aggregates is one of the main causes of the depletion of natural resources, as aggregates are constituents of several construction materials. Alternatively, it is, today, proven to be feasible to use mining tailings, either natural or recycled materials, to produce artificial aggregates through specific processes. A possible way to produce artificial aggregate is through the alkali activation of the powdered material in a process called geopolymerization. This study proposes to use a basalt powder and two different metakaolins as precursors for the production of an alkali-activated artificial aggregate, with a specific shape and size achieved by using 3D-printed molds. The experimental aggregates were evaluated using traditional tests for natural aggregates, such as resistance to compression, specific density and resistance to abrasion and fragmentation. Furthermore, the material was chemically analyzed in order to evaluate the geopolymerization process promoted by the two adopted metakaolins. The physical tests showed that artificial aggregates do not perform well in terms of resistance to wear and fragmentation, which can be improved. However, they revealed promising results in terms of skid, polishing and micro-texture.

Keywords: artificial aggregates; geopolymers; basalt powder; alkali-activated materials; polished stone value (PSV); micro-deval

1. Introduction

Natural aggregates mainly consist of crushed rock and sand coming from crushing bedrock or possibly from unconsolidated sand and gravel [1]. The widespread use of natural aggregates is one of the main causes of the depletion of natural resources, considering that aggregates are the basic constituent of several construction materials, such as bituminous and cementitious concretes. According to estimates for the year 2015, around 48 billion tons of natural aggregates was used worldwide, with a predicted growth rate of 5% every five years [2]. Thus, finding alternatives to natural aggregates is becoming crucial in the current scenario of sustainable transition that involves the construction industry [3,4]. The increasing need for sustainable construction materials is driving the research towards the reuse and recycling of waste to produce "recycled", "manufactured" and "artificial" aggregates [5]. The latest version of the EN 13242 standard [6] lists, in fact, recycled and manufactured aggregates among the aggregates that can be used in civil engineering work and road construction.

Recycled aggregates are classified as a result of the processing of inorganic or mineral material previously used in construction, while the manufactured ones come from an industrial process involving thermal or other modifications. To date, the most common example of recycled aggregates is represented by the Construction and Demolition Wastes (CDWs), which are processed to obtain recycled aggregates to partially or completely

substitute the natural aggregates for the production of construction materials [7]. On the other hand, there are several examples of manufactured aggregates, such as various slags or materials produced, involving thermal treatment of pumice, volcanic ashes, clays or siliceous rocks [8,9]. In the last few years, in addition to these mineral-based manufactured aggregates, an increasing number of by-products or wastes have been processed and treated to produce artificial aggregates (AAs) [10]. Unlike the processing of mineral-based materials, most of the solid wastes or industrial by-products must be pre-treated in order to eliminate the presence of potentially harmful substances. As an example, Incinerator Bottom Ashes (IBAs) contain heavy metals, chlorides, sulfates and other pollutants and must be pre-treated accordingly to be safely recycled and used as AAs [11]. However, despite the relatively long and expensive pre-treatment, the production of AAs contributes to the reduction in the exploitation of raw materials and represents potential economic and functional values for by-products and wastes [12,13]. Several by-products from different fields have been studied and experienced for the production of AAs, from coal bottom ash to crumb rubber, plastic waste and waste glass [14–19], and many others are still under investigation.

In terms of production methods, AAs generally come from a two-step procedure: granulation and hardening process [10]. The granulation process is widely adopted in different sectors (construction materials, food industry, pharmaceutical, etc.) and consists of the agglomeration of powdery substances to form grains or granules. The granulation technology for AA production generally requires the addition of liquid (wet granulation process) to create bonds between particles strong enough to bind them together and so enlarge their sizes. The following hardening step is needed to solidify the agglomerations to achieve specific mechanical properties. Based on the type of powder and the final application of the granules produced, different hardening technologies can be adopted. According to the most widespread applications of AAs, the most common hardening procedures are: sintering, cold bonding and alkali activation [10]. In the first process, the AAs are produced through a thermal treatment of the fresh granules at very high temperature (up to 1000 °C). The material undergoes an expansion and vitrification process, which allows for the strengthening of the granule. With the sintering being a chemical and physical process, the quality of the final AA, in terms of mechanical properties, is directly related to the chemical composition of the base material [19]. As a downside, this method has a significant impact in terms of emissions and energy consumption, due to the high temperature needed to run the process. On the contrary, the cold-bonding hardening technology is widely adopted considering the possibility to cure the AAs in water or at constant humidity. In this case, the strength of the granule is given by a pozzolanic reaction [20]. As a consequence, not every material is suitable for this process, with the pozzolanic reaction directly affected by the reactivity of the base material. The chemical reaction is also the core of the third mentioned hardening method: alkali activation. This is a chemical synthesis that occurs between silica and alumina-rich-based materials and strong alkali solutions, which allows for the development of ceramic materials [21]. In the production of AAs through this method, alkaline solutions, such as blends of sodium hydroxide and sodium silicate, are added as a binding agent as water replacement during the granulation process. Considering the relatively easy process and the absence of high temperatures for curing, the alkali activation of AAs is gaining popularity. Moreover, several studies verified the possibility of achieving high-performance AAs in terms of mechanical properties [22,23]. The application of geopolymeric AAs in cement concrete, in total or partial substitution of natural aggregates, is a current practice for buildings and pavements [24–27]. However, several applications have been carried out with the aim to substitute not only natural aggregates in construction materials but also add extra value to the final product. Fang et al. verified the feasibility of porous alkali-activated AAs carried for Phase Changing Material (PCM) to produce cement concrete to improve the energy efficiency of buildings [28] or asphalt concrete for pavements [29].

Following this trend of research, in the present paper, a preliminary laboratory characterization of AAs produced through the alkali activation of a basalt powder is presented. Even if the use of basalt for the formation of alkali-activated material has already been studied by different authors [30,31], the novelty of the present research is represented by the production process of AAs. The proposed basalt alkali-activated AAs are, in fact, cured in specific molds created with a 3D printer in order to have defined shapes and sizes, conceived to improve friction and acoustic properties when applied in the construction of road pavement wearing courses.

2. Materials and Methods

The geopolymer material is obtained from a mix of activators and precursors. Activators are alkaline liquids responsible for dissolving the precursors' structure and forming a brand-new structure. Precursors are usually aluminosilicate powders that, when dissolved in an alkaline solution, react and, depending on their origin, will provide different characteristics and proprieties to the final material. The geopolymer design might follow the trial-and-error method [32], mixing different precursors and activators' ratios, when the materials used as precursors constitute a heterogeneous and complex system and the involved chemical reactions are hard to predict in advance. However, it is possible to use theoretical basis to have a specific mix that allows for the geopolymers' production based on the chemical constitution of activators and precursors. In the following paragraphs, a basic characterization of the materials used in the experimental application is presented.

2.1. Precursors

Different precursors have been used in various research studies, among them fly ashes [33], metakaolin [34,35] and blast furnace slags [36]. The type of precursor has a direct impact on many mechanical and chemical properties of the geopolymer. Inert waste powder could act as a filler/aggregate in the geopolymer structure. On the other hand, a reactive amorphous waste could act as a precursor in the geopolymer matrix. Therefore, studying the precursors' mineralogy is vital to understand its constituent species and possible reactivity [37]. The materials used in this research as precursors were metakaolin and basalt in the shape of powder.

2.1.1. Basalt

Basalt powder is a by-product in the mining industry that has some commercial value. It can be used as a filler material [38] in fiber production or as a reactive part of the geopolymer mix [39,40]. In this research, the basalt powder used has 100% passing on the 0.063 mm sieve, with the following mineralogical composition, obtained by XRD analysis (Table 1).

Table 1. Chemical composition of the basalt powder (Reference Intensity Ratio (RIR) method).

Name	Composition	Percentage (%)
Leucite (L)	$(K(AlSi_2O_6))$	44
Augite (Au)	$((Ca,Mg,Fe)_2Si_2O_6)$	22
Anorthite (An)	$(Ca(Al_2Si_2O_8))$	11
Orthoclase (O)	$(K(AlSi_3O_8))$	5
Muscovite (M)	$(KAl_2(Si_3Al)O_{10}(OH)_2)$	5
Magnesiohornblendeferroan (Mh)	$(Ca_2(Mg_4Fe^{3+})(Si_7Al)O_{22}(OH)_2)$	4
Magnetite (Mt)	$(Fe^{2+}Fe^{3+}O_2)$	1

The XRD of the Basalt powder is shown in Figure 1, where it is possible to see the intensity of each material, as described in Table 1.
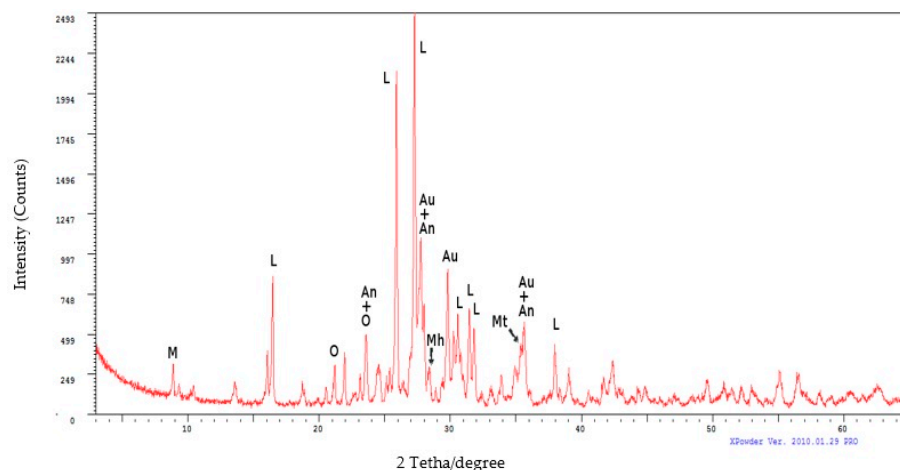
Figure 1. XRD of basalt powder.

Several researchers used basalt as a geopolymer material [31,37,38]. The data presented here demonstrate that the basalt powder has a sufficient amount of aluminum and silica. These indicate that the precursor is adequate to generate a geopolymer, as these minerals are responsible for the final geopolymer structure [32,39].

2.1.2. Metakaolin

Calcined kaolinitic clays, otherwise known as metakaolin (MK), were one of the first precursors used in geopolymer research. MK initial applications were mainly in paper and plastic industries, where it was used as filler. The composition of metakaolin is primarily made of SiO_2 and Al_2O_3 with a small percentage of metal oxides [32]. When used in cement concrete applications, MK increases the compressive and flexural strength of the concrete, reduces its permeability, increases its resistance to chemical attack, enhances the workability and increases the durability of the concrete [40]. Geopolymers can benefit from the MK qualities, especially as it has a high Al_2O_3 content, being very reactive with the activators [41–43]. In the present work, two distinct commercial metakaolin powders were used.

Based on XRD analysis for both the metakaolins, MK2 was found to be more reactive if compared to MK1, denoting the presence of amorphous reactive phases [34] and, thus, suitable to be used. On the other hand, MK1, even though it has an amorphous phase, has a crystal formation in it, probably due to some impurity originated in the production process, more likely to be a less calcinated kaolin (quartz-like structure).

2.2. Activators

The mixture of sodium silicate (SS) and sodium hydroxide (SH) creates a very basic NaOH solution, which is called activating fluid that allows for the dissolution of the aluminosilicates. It increases the pH and it compensates for the electric charge of the aluminates in the mixture. A 10M SH was used in the present work.

2.3. Research Plan

The characterization of artificial alkali-activated material is generally based on the characterizations of the alkali-activated paste and the characterization of the physical and mechanical properties of the produced aggregates. Due to the lack of specific tests for artificial alkali-activated aggregates, it was necessary to use the same methodologies adopted for aggregates of natural origin.

The characterization for the MK1/basalt mixture (Aggregate B-MK1) was reported in a previous study by the authors [31]. In that study, the authors proposed a regression equation that had as input the variables in the mixture (e.g., MK/basalt ration, liquid to solid ratio) and as a result the predicted Unified Compression Resistance. This regression

equation was applied for MK2/basalt mixture (Aggregate A-MK2). Results of compressive strength tests on cubic samples prepared with the alkali-activated paste, according to the EN10151-1 standard, are 35 MPa for the MK1 mix and 47 MPa for the MK2 one.

After the selection of the appropriate mixture design for both metakaolins, artificial-aggregates' samples were prepared through casting into the molds and curing, as shown in Figure 2. The A-MK2 aggregate passed through a second curing process to evaluate if it was possible to improve some properties. In this case, the aggregates underwent a second curing process of 24 h at 80 °C. The micro-Deval test after the second curing process was only performed on A-MK2 aggregates.
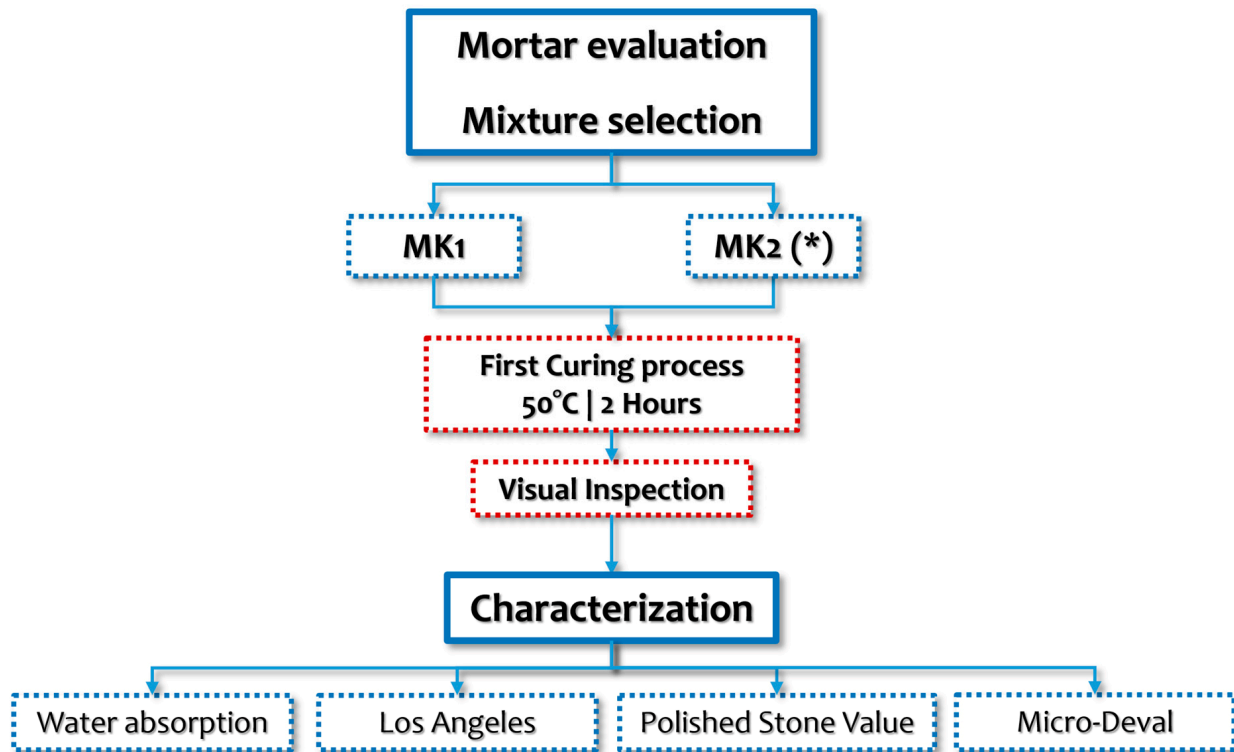
Figure 2. Flow chart of the production and testing process. (*) The MK2 aggregates underwent a second curing process of 24 h at 80 °C.

The molds were designed and printed with a 3D SLA printer to cast aggregates with a specific shape and size, aiming to reduce noise and increase friction in surface asphalt courses.

The aggregates were produced as described in a previous study [31], using the same mix proportions, with the used metakaolin being the only variable. Aggregate A was made with MK2 and Aggregate B with MK1.

2.4. Artificial Aggregate Production

The artificial aggregate was produced using 3D-printed molds that guarantee a specific shape and size that, according to [31,44], could have an interesting behavior in friction and acoustic prospects. The mixtures were prepared as described in Figure 3.
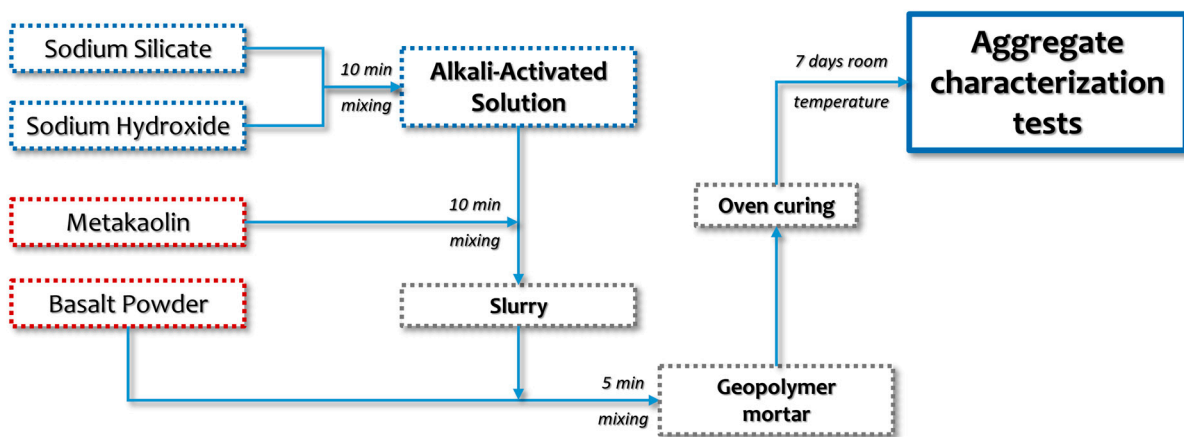
Figure 3. Flowchart of the artificial aggregate production.

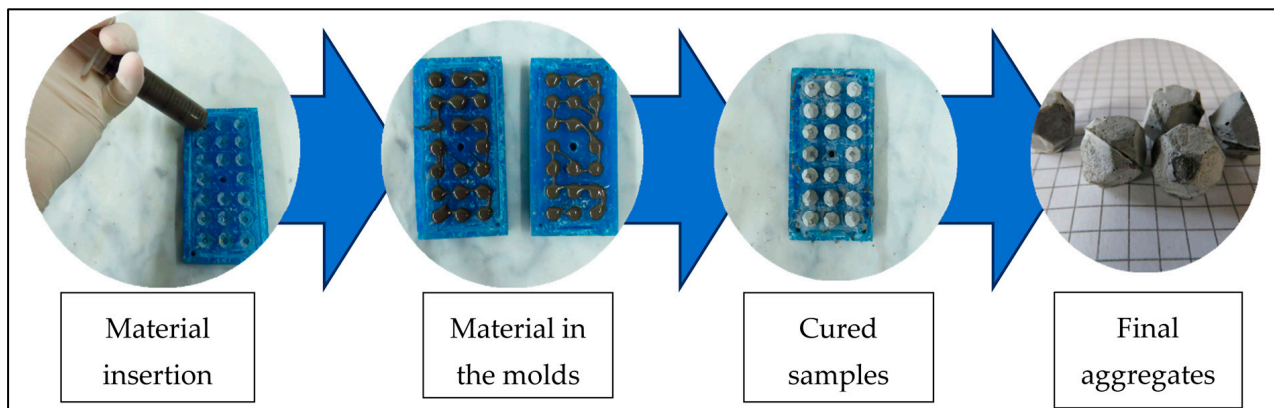The casting of the geopolymer mortar in the molds and the resulting aggregate are shown in Figure 4.

| Material insertion | Material in the molds | Cured samples | Final aggregates |

Figure 4. Process of artificial aggregate production using 3D-printed molds.

2.5. Artificial Aggregate Evaluation Methods

Both mixes were evaluated in terms of compressive strength in preliminary research [30] and subjected to X-Ray Diffraction (XRD) and Scanning Electron Microscopy (SEM). The produced aggregates were evaluated in terms of specific mass and water absorption following the EN 1097-6 Standard; Aggregate B-MK1 was submitted to EN 1097-2 for Los Angeles and EN1097-8 for Polished Stone Value (PSV), and both aggregates underwent EN-1097-1 for the micro-Deval.

Water absorption was determined according to the EN 1097-6 standard.

The Los Angeles (LA) test is an empirical measure of the resistance to fragmentation of mineral coarse aggregates used for pavement courses. A sample with a certain mass, depending on the particle size, is placed in a horizontal drum together with an appropriate number of steel balls. The drum is rotated for a total of 500 revolutions, during which the ball loads impact on the aggregates determining a fragmentation action, causing the formation of fine particles. The LA coefficient is obtained by the proportion of the fine particle mass created during the test and passing through a 1.6 mm sieve over the total mass of the sample [45].

The Polished Stone Value (PSV) test consists of evaluating the resistance of the aggregates against polishing action by a well-coded procedure. This test is carried out only for aggregates of specific dimension (7.2–10 mm), which are used only for asphalt wearing courses (EN 1097-8:2020). The polishing cycle has a duration of six hours, during which the polishing action is enhanced by using coarse abrasive sand and water for the first three

hours and fine abrasive sand and water for the last hours. The specimens for PSV test consist of manually and randomly placing the aggregates into the mold, making sure that the flat surface of each aggregate is properly matched with the mold surface, obtaining a single layer (Figure 5a).
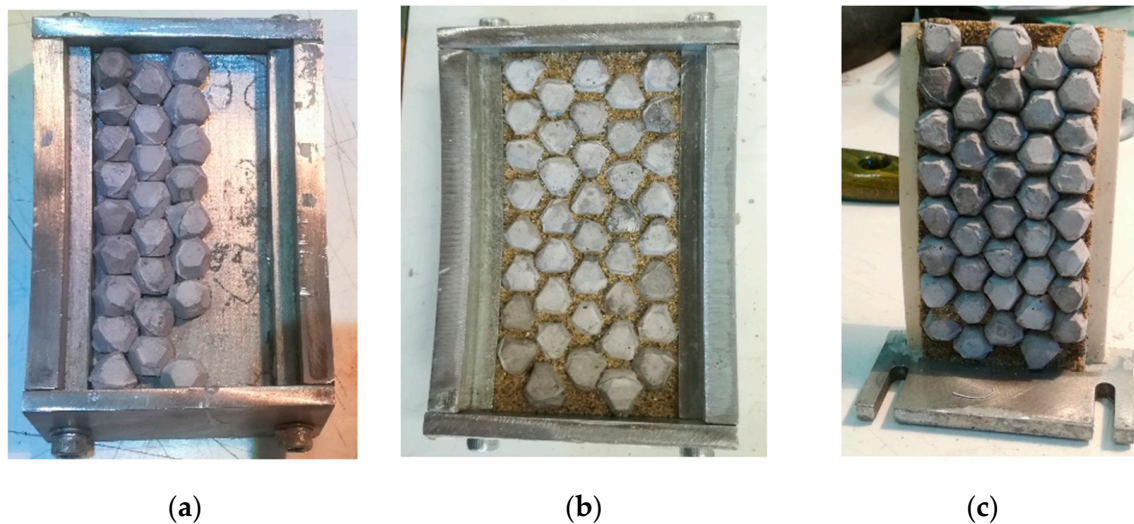

| (a) | (b) | (c) |

Figure 5. Sample preparation for the PSV test: (**a**) placement the aggregates in the mold; (**b**) aggregate mosaic completed before resin casting; (**c**) Mold completed.

Interstices between particles are filled with fine sand (Figure 5b) and then a bicomponent fiberglass is poured into the mold, in order to obtain a rigid sample once the resin hardens so that it preserves the mold curvature (Figure 5c).

For the case study, only the Aggregate B-MK1 (ID: B) was used for this test and as prescribed by the standard, it was compared with the basalt aggregate (ID: C). It is worth noting that, given the lack of a control stone recognized by the standard, a suitable alternative control stone of established PSV value was used [46]. The PSV was calculated according to the following standard equation.

$$PSV = S + X - C \qquad (1)$$

where:

- S is the mean value for the aggregate test specimens (Aggregate B-MK1);
- X is the mean PSV for the source of the control stone (in this case, 49);
- C is the mean value for the control stone specimens (basalt).

Furthermore, a roughness analysis was conducted on PSV specimens by means of a laser profilometer based on conoscopic holography methodology ISO 13473-3:2002. For each sample, five profiles were analyzed, two longitudinal profiles in the direction of the PSV wheel (a and b) and three in the crosswise direction (c, d and e), identified through the use of a mask (Figure 6). The alignments marked on the mask and a reference system defined for each sample help to carry out the profilometric analysis of aggregate surface texture before and after the PSV test. This ensures that the same profile is detected so that it can be completely superimposable with a reasonable approximation. Profiles were captured by means of a lens with an objective focal length of 50 mm and a sampling resolution of 5 µm.
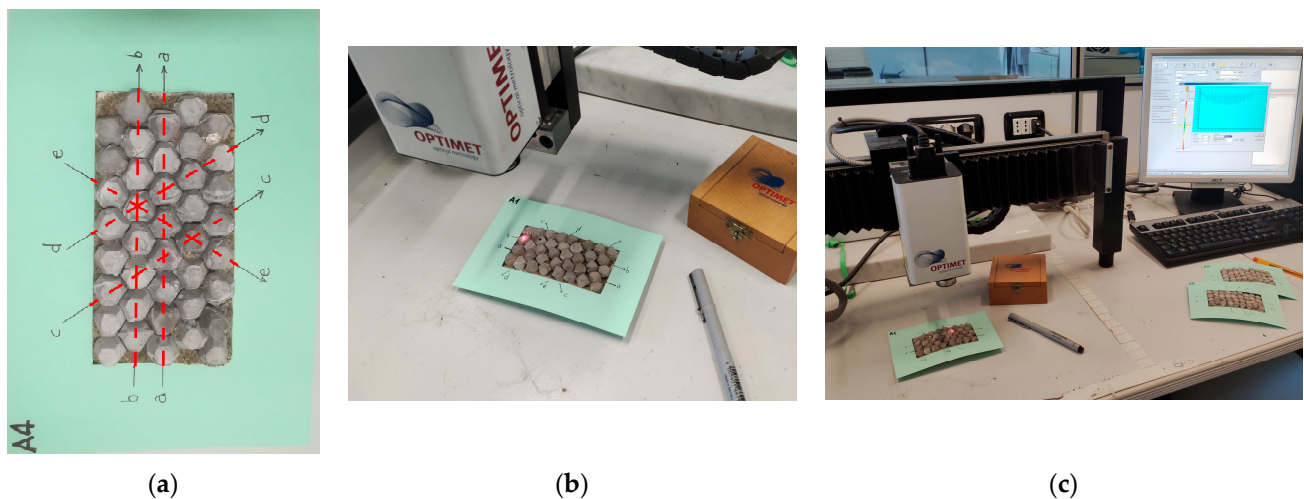
(**a**)

(**b**)

(**c**)

Figure 6. Roughness analysis by laser profilometer: (**a**) Alignment's identification mask; (**b**,**c**) in action for the micro-texture measurement.

The estimated micro-texture indexes (see Table 2) are defined as follows:

I.   Ra: arithmetical mean deviation roughness of the profile, which represents an average of the profile deviations from a center line;
II.   Rq: root mean squared roughness;
III.   Rz: average peak-to-valley height, which is based on the five highest peaks and the lowest valleys over the entire length of the evaluation segment [47]

Table 2. Formulas and graphical explanation of the investigated roughness indicators.

Roughness Indicator	R_a	R_q	R_z
Formula	$R_a = \frac{1}{n} \cdot \sum_{i=1}^{n} |y_i|$	$R_q = \sqrt{\frac{1}{n} \cdot \sum_{i=1}^{n} y_i^2}$	$R_z = \frac{1}{5} \cdot \sum_{i=1}^{5} R_{pi} - R_{vi}$
Graphical Explanation			

The last test carried out was the micro-Deval (EN 1097-1), which evaluates the resistance to wear of coarse aggregates. The test provides a measure of aggregate abrasion resistance by means of an abrasive action that occurs between the aggregates themselves and the aggregates and small steel balls in the presence of water. A 500 g sample is placed together with 2.5 liters of water and an abrasive charge, consisting of a set number of steel balls, inside a specific apparatus that is rotated for 12,000 revolutions. After the test, the sample is removed from the drum, washed and the oversize fraction retained on a 1.6 mm sieve is dried. The micro-Deval coefficient (MDE) is calculated by the difference between the initial mass and the oversized fraction mass compared to the total mass of the sample.

3. Results

3.1. Alkali-Activated Materials' Chemical Characterization

The characterization of the alkali-activated materials was conducted using XRD and SEM, for both mixes. The analysis of SEM images allows for the identification of the formation of geopolymer gel. Furthermore, with the XRD, it is possible to identify the geopolymerization region and some of the crystals that did not react.

From the XRD image in Figure 7, it is possible to notice that a reaction occurred due to the alkaline activation of the precursors, given the hump between 20 and 30 2θ recorded on the spectra, compared to that of the constituent materials. This suggests the formation of geopolymeric structures, as observable in the SEM images. The crystalline phases detected in both samples derive from unreacted basalt and metakaolin. As expected, no new crystalline phases were formed.
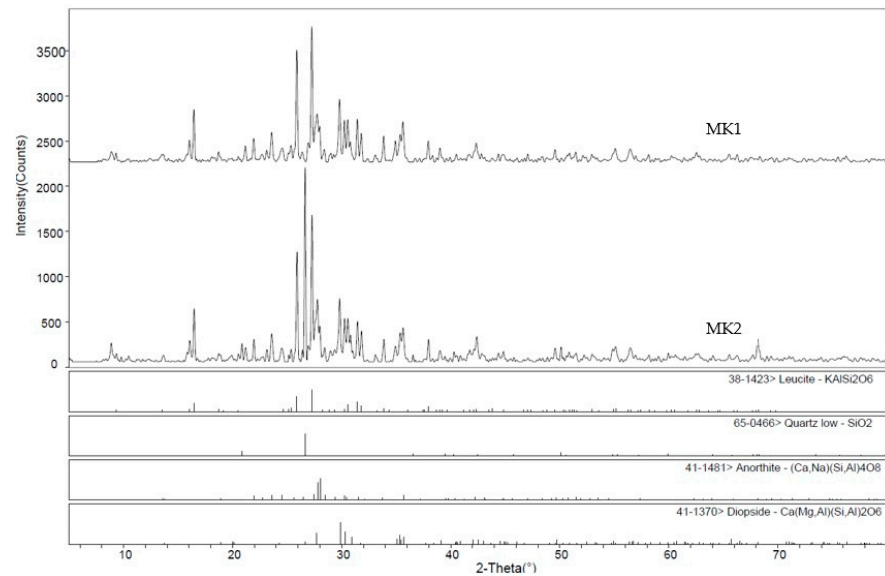

Figure 7. XRD for geopolymer mixes containing different metakaolins (MK, MK2).

Figure 8 shows, at 10,000 magnification, the internal part of Aggregate A and Aggregate B, with these mixes made with MK2 and MK1 metakaolin, respectively.

Aggregate A
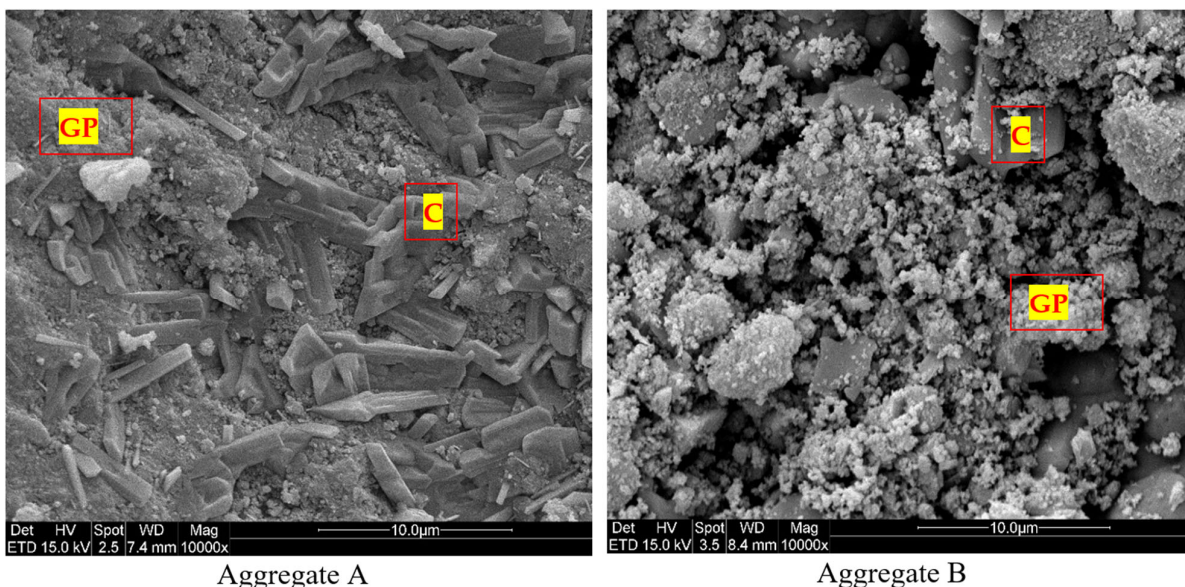
Aggregate B

Figure 8. SEM images of the geopolymer Aggregate A and Aggregate B.

In both materials, it is possible to see the formation of a geopolymer gel (GP) and the presence of crystals of different mineral phases from unreacted precursors (C). The most notable difference is that in the MK2 mix, the geopolymer gel is more homogeneous and compact, and the unreacted crystalline phases from basalt are well incorporated into the geopolymer matrix. In the other mix, the geopolymer formation resulted in a less cohesive material, with typical nanoprecipitates formed by alkali activation, unevenly disposed

around the unreactive phases of both precursors. The scarce reactivity of MK1, deriving from the presence of fewer readily reactive amorphous phases and its coarser particle size, resulted in a highly porous and less compacted material, likely having lower physical and mechanical properties.

3.2. Artificial Aggregate Characterization

Aggregate A and Aggregate B were characterized in terms of water content, specific mass, Los Angeles abrasion, Polished Stone Value and micro-Deval abrasion. Table 3 shows the results for both artificial aggregate types and their direct comparison with a natural aggregate (basalt), two artificial aggregates that follow a different production method, (i.e., calcined Bauxite and steel slag) and an AA produced through the alkali activation of fly ashes.

Table 3. Materials' characteristics and comparison with other aggregates.

Aggregate	Water Content (%)	Specific Mass (g/cm^3)	Los Angeles (%)	PSV	Micro-Deval (%)	Reference
Aggregate A	19.1	2.120	-	-	35 * (27)	-
Aggregate B	21.0	2.017	37	59	70	-
Basalt	<2.5	2.700	14–20	53	14	[48–50]
Calcined Bauxite	6.8	2.629	10–17	50–70	5	[48,51,52]
Fly ash AA	5.5	2.140	27	-	-	[53]
Steel slag	1.1–9.0	2.96–3.59	14–15	25–55	6–10	[47,54]

* Results after treating the material in the oven for 24 h at 80 °C, after previous curing.

It is important to note that both artificial aggregates produced in this research have a higher water content than the aggregates used as a reference. It is important to note that natural aggregates, such as basalt, typically have less water absorption. Regarding the calcined bauxite and steel slag, which are not geopolymer materials, the internal structure is different and, thus, can contribute to different water absorption. As for the fly ash AA, even though it is a geopolymer artificial aggregate, the production process is quite different. The different production process and use of fly ash can be contributors to the difference in the water absorption. The specific mass is comparable to the fly ash AA one.

The artificial aggregate B had high results in terms of Los Angeles and micro-Deval abrasion tests; however, promising results were obtained from PSV. Aggregate A was not tested in terms of Los Angeles and PSV. However, its micro-Deval was considerably better than the one for aggregate B, especially if the material was heat-treated in the oven after the initial curing.

3.3. Artificial Aggregate Micro-Texture Analysis

As for the micro-texture characterization, the analysis was carried out for the Aggregate B-MK1 and the control basalt. Data were obtained by analyzing micro-profiles of an average length of 0.7–1.05 mm, graphically identified on each single grain that composes a profile. For Aggregate B-MK1, a total of 119 micro-profiles with an average length of 909 μm was analyzed, whereas for the control basalt, 120 micro-profiles with an average length of 834 μm were recorded.

Table 4 shows the results of the micro-texture analysis, where the collected data for each aggregate were averaged for longitudinal and crosswise profiles, for both polished and unpolished samples. The percentage variation in roughness data Ri (with i = a, q, z) registered before (Ri,bp) and after (Ri,ap) polishing is given by:

$$\Delta R_i = \frac{R_{i,ap} - R_{i,bp}}{R_{i,bp}} \cdot 100 \tag{2}$$

Table 4. Post-processing analysis of roughness data collected by laser profilometer: mean values before and after polishing and variation (%).

ID Sample:	Data	Before Polishing (μm)			After Polishing (μm)			Variation (%)		
		$R_{a,bp}$	$R_{q,bp}$	$R_{z,bp}$	$R_{a,ap}$	$R_{q,ap}$	$R_{z,ap}$	ΔR_a	ΔR_q	ΔR_z
Aggregate B-MK1 (B)	Longitudinal sections (mean)	12.6	16.8	50.9	19.6	24.4	69.1	+88.9	+78.0	+60.1
	Crosswise sections (mean)	9.5	12.6	40.9	25.4	30.9	79.1	+173.4	+151.6	+94.5
	Mean	10.7	14.3	45.0	23.1	28.3	75.1	+127.7	+111.1	+75.4
Control Basalt (C)	Longitudinal sections (mean)	24.8	30.6	75.7	26.3	32.5	84.7	+6.1	+6.5	+14.3
	Crosswise sections (mean)	22.3	27.5	67.9	27.0	32.9	80.0	+21.2	+20.0	+17.9
	Mean	23.3	28.7	71.0	26.7	32.8	81.9	+14.7	+14.0	+15.8

As it can be clearly seen from Table 4, Aggregate B-MK1 shows an important increase in the micro-texture indexes, almost doubling in value, whereas the basalt exhibits a lower variation, 15% on average, which can be considered not significant. This is in line with other studies carried out by means of a similar methodology, which recorded low variation in the basalt aggregates in terms of roughness [47,48].

In addition, profile tracking with the laser profilometer provided the basis to conduct further analysis on the samples in order to obtain more information about the wearing characteristics of the materials. Thus, the percentage of loss material was estimated starting with the calculation of the area underneath the profiles (*Aap*: area after polishing; *Abp*: area before polishing) by means of the trapezoid method, with a step of 5 μm, which is given by the following formula:

$$\Delta A = \frac{A_{ap} - A_{bp}}{A_{bp}} \cdot 100 \tag{3}$$

Table 5 summarizes the percentage of loss material estimated for the longitudinal and the crosswise sections after submitting the samples to the PSV abrasion. Figures 9 and 10 show an example of the profile's superposition for both the Aggregate B-MK1 (A6 sample) and the Control Basalt (C2 sample), respectively. It can be clearly seen that the artificial aggregates have undergone a significant loss in material due to the polishing, whereas the basalt profiles appear to be almost unaltered.

Table 5. Percentage estimation of the material loss occurring after the polishing action.

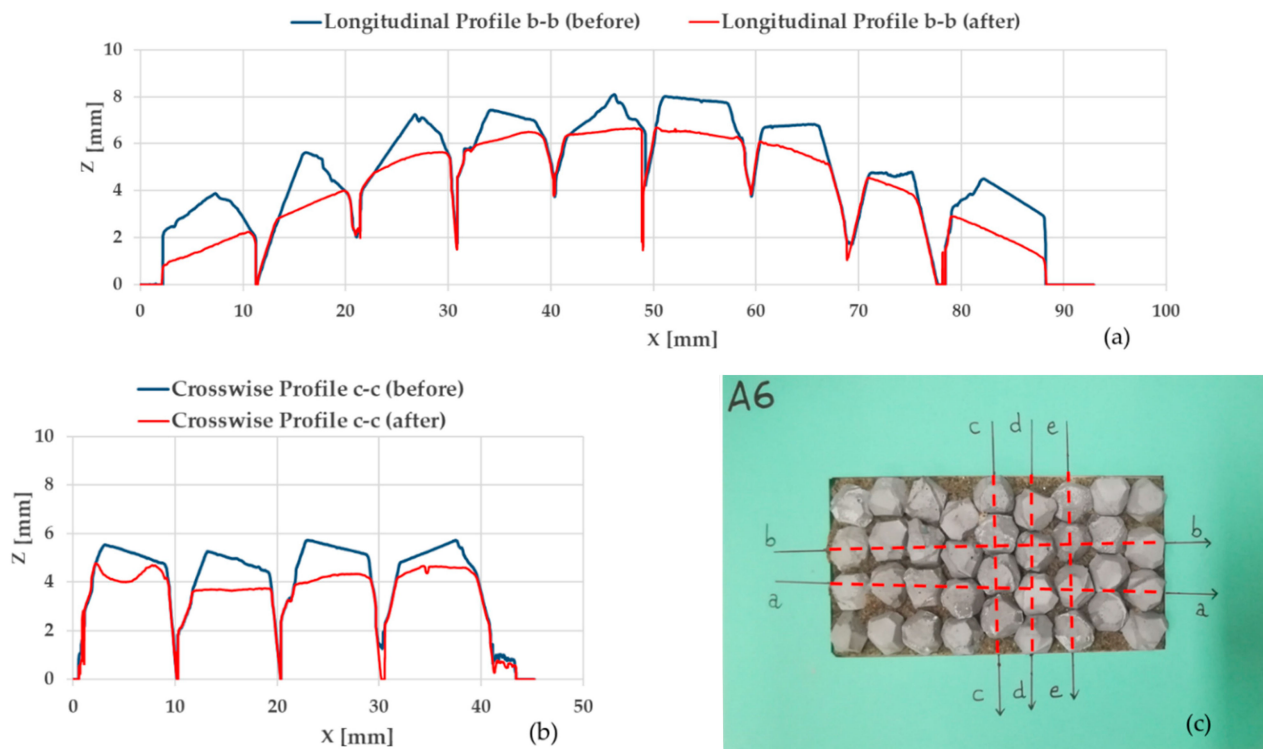| ID Sample: Aggregate B-MK1 (B)	ΔA Variation (%)	St. Dev (%)
Longitudinal sections (mean)	−16.9	±4.5
Crosswise sections (mean)	−17.4	±2.1
ID Sample: Control Basalt (C)	**ΔA Variation (%)**	**St. Dev (%)**
Longitudinal sections (mean)	−3.7	±1.4
Crosswise sections (mean)	−4.1	±1.0

Figure 9. Example of the profile's superposition for Aggregate B-MK: longitudinal profile (**a**) and crosswise profile (**b**); alignment's identification mask for A6 sample (**c**).
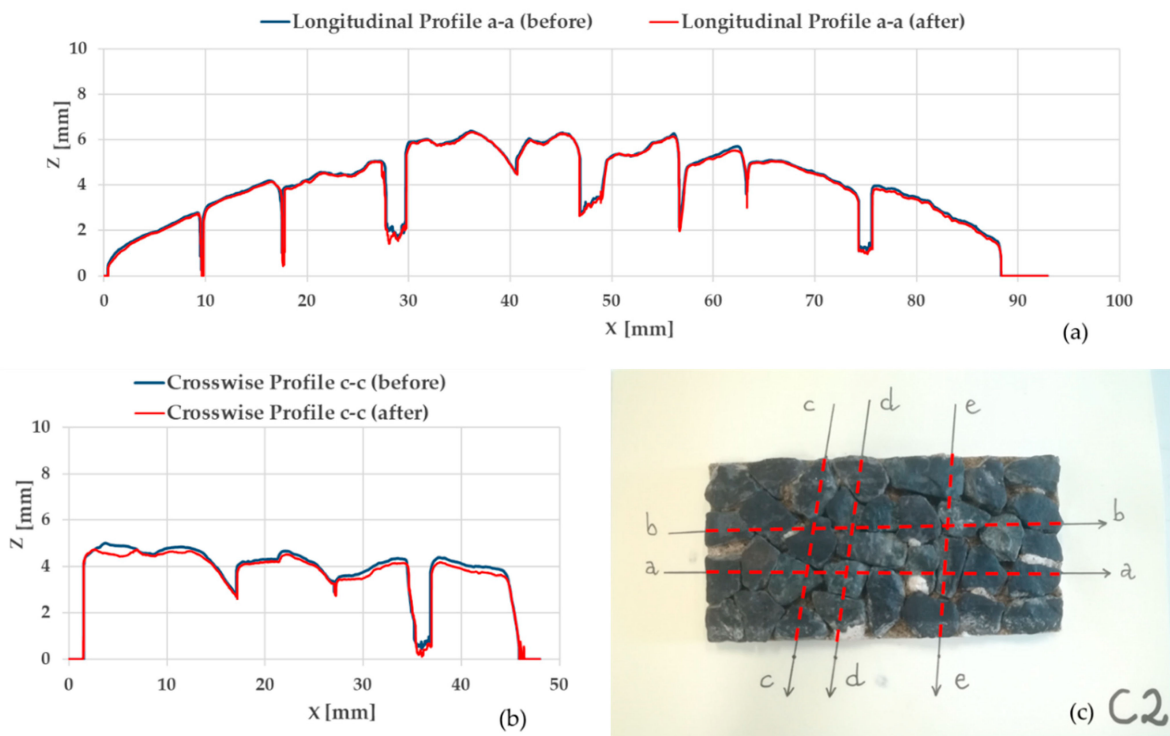

Figure 10. Example of the profile's superposition for control basalt: longitudinal profile (**a**) and crosswise profile (**b**); alignment's identification mask for C2 sample (**c**).

Skid resistance results obtained by means of the British Pendulum Test are shown in Table 6, where PTV_b is the British Pendulum value measured on unpolished samples, whereas PTV_a is the measurement after the polishing action. Aggregate B-MK1 kept high values of PTV, showing a variation of about -10% on average after the polishing, whereas the control basalt samples showed almost a doubled percentage variation (-18.3%).

Table 6. Results of the PSV test: Pendulum Test Value (PTV) before and after polishing, percentage variation and PSV values.

ID Sample	PTV_b	PTV_a	Variation (%)	PSV
Aggregate B-MK1 (B)	62	56	−9.9	59.0
Control Basalt (C)	56	46	−18.3	49.0

Based on the results, it is possible to state that the basalt kept a similar value between pre and post-polishing (Tables 3 and 4) on average and did not suffer the effects due to the polishing also in terms of loss of material. Instead, the Aggregate B-MK1 showed a significant increase in all the micro-texture indexes after the polishing. This might also be due to the initially smooth surface finishing, with the aggregates cast and cured in a mold, whereas the polishing action let the crystals (Figure 9) rise to the surface. Despite maintaining a high value of PTV after conditioning, the artificial aggregates exhibited a great loss in terms of material, which corresponded to a remodeling of the macro-texture of the samples, obtaining a quite different contact area between the surface of the sample and the pad of the British Pendulum.

4. Conclusions

This research aimed at the preliminary characterization of engineered artificial aggregates produced through the alkali activation of basalt and metakaolin powders.

The main goal was to conduct a preliminary evaluation of the artificially engineered aggregate. The AEA was evaluated in terms of resistance to abrasion, fragmentation, water absorption and polishing. The main conclusions are as follows:

- It was noted that the selected metakaolin played a very important role, as the MK2 one had better geopolymerization results.
- The basalt powder proved to be a suitable material.
- The AEA with MK2 had a higher resistance to wear than the one with MK1.
- The post-curing heat treatment improves the material characteristics.
- The PSV and BPN results are quite promising, showing that it might be used in replacement of natural aggregate or other artificial aggregates.
- The process must be improved in order to increase the overall quality of the AEA, especially in terms of fragmentation results.

As for the basalt action as a constituent, it is clear that it did not fully react. Part of it contributed to the geopolymerization and partly acted as a non-reactive material (filler), as evidenced by the crystals in Figure 9. However, more research is necessary to better understand its contribution to the geopolymerization process in a multi-material system along with metakaolin.

Regarding the physical characterization, the aggregate B-MK1 showed lower results in most tests compared to the reference materials (i.e., basalt, calcined Bauxite, fly ash AA, steel slags), except for the PSV. However, despite the fact that the artificial aggregate does not perform well in those tests, it revealed high PTV values and optimal micro-texture indexes.

By changing the metakaolin in aggregate A-MK2, the resistance to wear increased, halving the loss of material due to the abrasive action. It appears that the results improved even further in terms of micro-Deval coefficient when the artificial aggregates were heat-treated.

Therefore, although the mixture requires improvements in order to achieve a better behavior in terms of resistance to wear and fragmentation, the high PTV and PSV values,

as well as the quality of micro-texture indexes, are proof of potential good performance, making the artificial aggregates suitable as a replacement of natural aggregates for wearing courses in road pavements.

All in all, the research shows that producing artificial geopolymer aggregates using 3D-printed molds to control their shape and size is a promising approach that could be scaled to larger industrial productions. It is necessary to evaluate the possibility to 3D print the aggregates and not only the molds, which could increase the production process, especially in an industrial context.

Future developments will foresee a complete characterization of aggregate A that will be used for the production of microsurfacing mixes to evaluate its behavior in friction and acoustic terms.

Author Contributions: Conceptualization, S.C.C., P.T. and C.S.; methodology, S.C.C.; software, S.C.C., M.D.R. and A.N.M., writing original draft preparation, S.C.C.; writing—review and editing, M.D.R., A.N.M., R.V., P.T. and C.S.; supervision, C.S. All authors have read and agreed to the published version of the manuscript.

Conflicts of Interest: The authors declare no conflict of interest.

References

1. Langer, W. 9—Sustainability of aggregates in construction. In *Sustainability of Construction Materials*, 2nd ed.; Khatib, J.M., Ed.; Woodhead Publishing Series in Civil and Structural Engineering; Woodhead Publishing: Sawston, UK, 2016; pp. 181–207. ISBN 978-0-08-100995-6.
2. The Freedonia Group. Global Demand for Construction Aggregates to Exceed 48 Billion Metric Tons in 2015. Available online: https://www.freedoniagroup.com/World-Construction-Aggregates.html (accessed on 1 May 2021).
3. Akhtar, A.; Sarmah, A.K. Construction and demolition waste generation and properties of recycled aggregate concrete: A global perspective. *J. Clean. Prod.* **2018**, *186*, 262–281. [CrossRef]
4. Zabalza Bribián, I.; Valero Capilla, A.; Aranda Usón, A. Life cycle assessment of building materials: Comparative analysis of energy and environmental impacts and evaluation of the eco-efficiency improvement potential. *Build. Environ.* **2011**, *46*, 1133–1140. [CrossRef]
5. Chen, W.; Jin, R.; Xu, Y.; Wanatowski, D.; Li, B.; Yan, L.; Pan, Z.; Yang, Y. Adopting recycled aggregates as sustainable construction materials: A review of the scientific literature. *Constr. Build. Mater.* **2019**, *218*, 483–496. [CrossRef]
6. *EN 13242:2015*; Aggregates for Unbound and Hydraulically Bound Materials for Use in Civil Engineering Work and Road Construction. European Committee for Standardization (CEN): Brussels, Belgium, 2015.
7. Bai, G.; Zhu, C.; Liu, C.; Liu, B. An evaluation of the recycled aggregate characteristics and the recycled aggregate concrete mechanical properties. *Constr. Build. Mater.* **2020**, *240*, 117978. [CrossRef]
8. Aslam, M.S.; Huang, B.; Cui, L. Review of construction and demolition waste management in China and USA. *J. Environ. Manag.* **2020**, *264*, 110445. [CrossRef] [PubMed]
9. Behera, M.; Bhattacharyya, S.K.; Minocha, A.K.; Deoliya, R.; Maiti, S. Recycled aggregate from C&D waste & its use in concrete—A breakthrough towards sustainability in construction sector: A review. *Constr. Build. Mater.* **2014**, *68*, 501–516.
10. Ren, P.; Ling, T.-C.; Mo, K.H. Recent advances in artificial aggregate production. *J. Clean. Prod.* **2021**, *291*, 125215. [CrossRef]
11. Colangelo, F.; Messina, F.; Cioffi, R. Recycling of MSWI fly ash by means of cementitious double step cold bonding pelletization: Technological assessment for the production of lightweight artificial aggregates. *J. Hazard. Mater.* **2015**, *299*, 181–191. [CrossRef]
12. Tajra, F.; Abd Elrahman, M.; Lehmann, C.; Stephan, D. Properties of lightweight concrete made with core-shell structured lightweight aggregate. *Constr. Build. Mater.* **2019**, *205*, 39–51. [CrossRef]
13. Tajra, F.; Elrahman, M.A.; Stephan, D. The production and properties of cold-bonded aggregate and its applications in concrete: A review. *Constr. Build. Mater.* **2019**, *225*, 29–43. [CrossRef]
14. Balapour, M.; Zhao, W.; Garboczi, E.J.; Oo, N.Y.; Spatari, S.; Hsuan, Y.G.; Billen, P.; Farnam, Y. Potential use of lightweight aggregate (LWA) produced from bottom coal ash for internal curing of concrete systems. *Cem. Concr. Compos.* **2020**, *105*, 103428. [CrossRef]
15. Qaidi, S.M.A.; Dinkha, Y.Z.; Haido, J.H.; Ali, M.H.; Tayeh, B.A. Engineering properties of sustainable green concrete incorporating eco-friendly aggregate of crumb rubber: A review. *J. Clean. Prod.* **2021**, *324*, 129251. [CrossRef]
16. Saikia, N.; de Brito, J. Use of plastic waste as aggregate in cement mortar and concrete preparation: A review. *Constr. Build. Mater.* **2012**, *34*, 385–401. [CrossRef]
17. Liu, Y.; Shi, C.; Zhang, Z.; Li, N. An overview on the reuse of waste glasses in alkali-activated materials. *Resour. Conserv. Recycl.* **2019**, *144*, 297–309. [CrossRef]

18. Valášková, M.; Blahůšková, V.; Vlček, J. Effects of Kaolin Additives in Fly Ash on Sintering and Properties of Mullite Ceramics. *Minerals* **2021**, *11*, 887. [CrossRef]
19. Yue, M.; Yue, Q.Y.; Qi, Y.F. Effect of Sintering Temperature on the Properties of Sludge Ceramics and Fly-Ash Ceramics. In *Advanced Materials Research*; Trans Tech Publications Ltd: Bäch, Switzerland, 2011; Volume 150, pp. 1068–1072.
20. Tang, P.; Xuan, D.; Poon, C.S.; Tsang, D.C.W. Valorization of concrete slurry waste (CSW) and fine incineration bottom ash (IBA) into cold bonded lightweight aggregates (CBLAs): Feasibility and influence of binder types. *J. Hazard. Mater.* **2019**, *368*, 689–697. [CrossRef]
21. Khale, D.; Chaudhary, R. Mechanism of geopolymerization and factors influencing its development: A review. *J. Mater. Sci.* **2007**, *42*, 729–746. [CrossRef]
22. Morone, M.; Costa, G.; Georgakopoulos, E.; Manovic, V.; Stendardo, S.; Baciocchi, R. Granulation–Carbonation Treatment of Alkali Activated Steel Slag for Secondary Aggregates Production. *Waste Biomass Valorization* **2017**, *8*, 1381–1391. [CrossRef]
23. Bui, L.A.; Hwang, C.; Chen, C.; Lin, K.; Hsieh, M. Manufacture and performance of cold bonded lightweight aggregate using alkaline activators for high performance concrete. *Constr. Build. Mater.* **2012**, *35*, 1056–1062. [CrossRef]
24. Gopalakrishna, B.; Dinakar, P. Mix design development of fly ash-GGBS based recycled aggregate geopolymer concrete. *J. Build. Eng.* **2022**, *63*, 105551. [CrossRef]
25. Saloni; Parveen; Lim, Y.Y.; Pham, T.M. Effective utilisation of ultrafine slag to improve mechanical and durability properties of recycled aggregates geopolymer concrete. *Clean. Eng. Technol.* **2021**, *5*, 100330. [CrossRef]
26. Zheng, Y.; Xiao, Y.; Wang, C.; Li, Y. Behavior of square geopolymer recycled brick aggregate concrete filled steel tubular stub columns under axial compression. *Constr. Build. Mater.* **2022**, *363*, 129823. [CrossRef]
27. Wongkvanklom, A.; Posi, P.; Kampala, A.; Kaewngao, T.; Chindaprasirt, P. Beneficial utilization of recycled asphaltic concrete aggregate in high calcium fly ash geopolymer concrete. *Case Stud. Constr. Mater.* **2021**, *15*, e00615. [CrossRef]
28. Fang, Y.; Ahmad, M.R.; Lao, J.C.; Qian, L.P.; Dai, J.D. Development of artificial geopolymer aggregates with thermal energy storage capacity. *Cem. Concr. Compos.* **2022**, *135*, 104834. [CrossRef]
29. Zhou, X.; Kastiukas, G.; Lantieri, C.; Tataranni, P.; Vaiana, R.; Sangiorgi, C. Mechanical and thermal performance of macro-encapsulated phase change materials for pavement application. *Materials* **2018**, *11*, 1398. [CrossRef]
30. Ismaiel Saraya, M.E.-S.; El-Fadaly, E. Preliminary Study of Alkali Activation of Basalt: Effect of NaOH Concentration on Geopolymerization of Basalt. *J. Mater. Sci. Chem. Eng.* **2017**, *5*, 58–76. [CrossRef]
31. Callai, S.C.; Tataranni, P.; Sangiorgi, C. Preliminary evaluation of geopolymer mix design applying the design of experiments method. *Infrastructures* **2021**, *6*, 35. [CrossRef]
32. Davidovits, J. *Geopolymer Chemistry and Application*, 4th ed.; Institut Geopolymere: Saint-Quentin, France, 2015.
33. Liu, Z.; Cai, C.S.; Liu, F.; Fan, F. Feasibility Study of Loess Stabilization with Fly Ash–Based Geopolymer. *J. Mater. Civ. Eng.* **2016**, *28*, 04016003. [CrossRef]
34. Moro, D.; Fabbri, R.; Romano, J.; Ulian, G.; Calafato, A.; Solouki, A.; Sangiorgi, C.; Valdrè, G. Thermal, X-ray Diffraction and Oedometric Analyses of Silt-Waste/NaOH-Activated Metakaolin Geopolymer Composite. *J. Compos. Sci.* **2021**, *5*, 269. [CrossRef]
35. Solouki, A.; Viscomi, G.; Lamperti, R.; Tataranni, P. Quarry waste as precursors in geopolymers for civil engineering applications: A decade in review. *Materials* **2020**, *13*, 3146. [CrossRef]
36. Jiao, X.; Zhang, Y.; Chen, T.; Bao, S.; Liu, T.; Huang, J. Geopolymerisation of a silica-rich tailing. *Miner. Eng.* **2011**, *24*, 1710–1712. [CrossRef]
37. Rill, E.; Lowry, D.R.; Kriven, W.M. Properties of basalt fiber reinforced geopolymer composites. *Ceram. Eng. Sci. Proc.* **2010**, *31*, 57–67. [CrossRef]
38. Tataranni, P.; Besemer, G.M.; Bortolotti, V.; Sangiorgi, C. Preliminary research on the physical and mechanical properties of alternative lightweight aggregates produced by alkali-activation of waste powders. *Materials* **2018**, *10*, 1255. [CrossRef]
39. Provis, J.L.; Rees, C. *Geopolymers: Structures, Processing, Properties and Industrial Applications*; Elsevier: Amsterdam, The Netherlands, 2009.
40. Siddique, R.; Klaus, J. Influence of metakaolin on the properties of mortar and concrete: A review. *Appl. Clay Sci.* **2009**, *43*, 392–400. [CrossRef]
41. Longhi, M.A.; Rodríguez, E.D.; Walkley, B.; Zhang, Z.; Kirchheim, A.P. Metakaolin-based geopolymers: Relation between formulation, physicochemical properties and efflorescence formation. *Compos. Part B Eng.* **2020**, *182*, 107671. [CrossRef]
42. Aboulayt, A.; Riahi, M.; Ouazzani Touhami, M.; Hannache, H.; Gomina, M.; Moussa, R. Properties of metakaolin based geopolymer incorporating calcium carbonate. *Adv. Powder Technol.* **2017**, *28*, 2393–2401. [CrossRef]
43. Medri, V.; Papa, E.; Lizion, J.; Landi, E. Metakaolin-based geopolymer beads: Production methods and characterization. *J. Clean. Prod.* **2020**, *244*, 118844. [CrossRef]
44. Copetti Callai, S.; Sangiorgi, C. A review on acoustic and skid resistance solutions for road pavements. *Infrastructures* **2021**, *6*, 41. [CrossRef]
45. Artoni, R.; Cazacliu, B.; Hamard, E.; Cothenet, A.; Parhanos, R.S. Resistance to fragmentation of recycled concrete aggregates. *Mater. Struct. Constr.* **2017**, *50*, 11. [CrossRef]
46. Dunford, A. *Establishing a New Supply of UK PSV Control Stone Including Results of Supplementary Experiments*; Published Project Report PPR603; Transport Research Laboratory: Crothon, UK, 2013; p. 20.

47. Vaiana, R.; Balzano, F.; Iuele, T.; Gallelli, V. Microtexture performance of EAF slags used as aggregate in asphalt mixes: A comparative study with surface properties of natural stones. *Appl. Sci.* **2019**, *9*, 3197. [CrossRef]

48. Woodward, D.; Friel, S. Predicting the wear of high friction surfacing aggregate. *Coatings* **2017**, *7*, 71. [CrossRef]

49. Czinder, B.; Vásárhelyi, B.; Török, Á. Long-term abrasion of rocks assessed by micro-Deval tests and estimation of the abrasion process of rock types based on strength parameters. *Eng. Geol.* **2021**, *282*, 105996. [CrossRef]

50. Korkanç, M.; Tuğrul, A. Evaluation of selected basalts from Nĭde, Turkey, as source of concrete aggregate. *Eng. Geol.* **2004**, *75*, 291–307. [CrossRef]

51. Li, S.; Xiong, R.; Dong, X.; Sheng, Y.; Guan, B.; Zong, Y.; Xie, C.; Zhai, J.; Li, C. Effect of chemical composition of calcined bauxite aggregates on mechanical and physical properties for high friction surface course. *Constr. Build. Mater.* **2021**, *302*, 124390. [CrossRef]

52. Manaf, M.B.H.A.; Abdul Razak, R.; Muhamad, K.; Abdul Rahim, M.; Ahmad, M.M.; Hao, T.P. A study on the potential of geopolymer artificial aggregate as substitute for granite and limestone aggregate. *IOP Conf. Ser. Earth Environ. Sci.* **2020**, *476*, 012034. [CrossRef]

53. Li, S.; Xiong, R.; Yu, D.; Zhao, G.; Cong, P.; Jiang, Y. *Friction Surface Treatment Selection: Aggregate Properties, Surface Characteristics, Alternative Treatments, and Safety Effects*; Purdue University: West Lafayette, IN, USA, 2017; ISBN 9781622604784.

54. Mohajerani, A.; Suter, D.; Jeffrey-Bailey, T.; Song, T.; Arulrajah, A.; Horpibulsuk, S.; Law, D. Recycling waste materials in geopolymer concrete. *Clean Technol. Environ. Policy* **2019**, *21*, 493–515. [CrossRef]